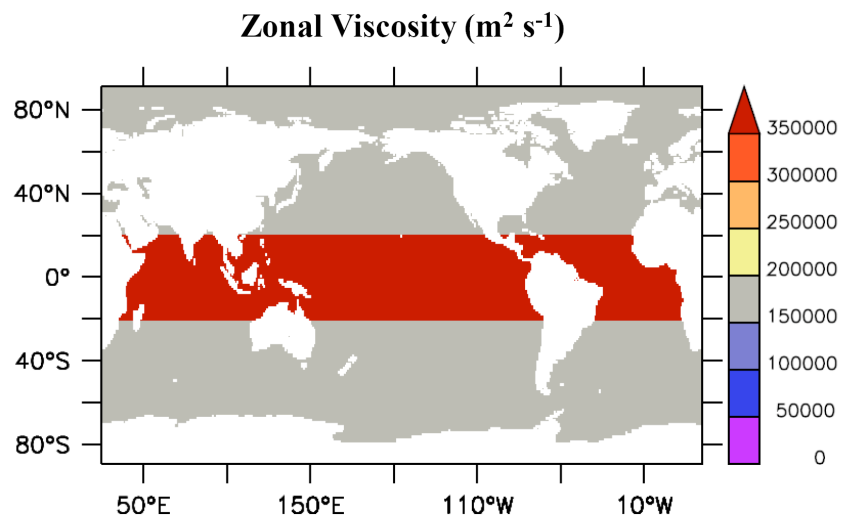
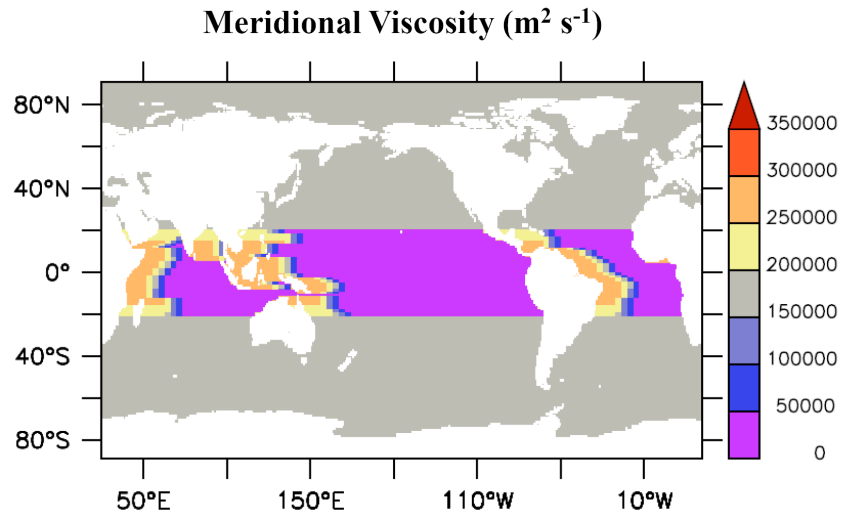


1 **Supplementary Material 1: Anisotropic Viscosity Scheme**

2 Horizontal viscosity is required in ocean circulation models to resolve the western boundary  
3 currents and to smooth out numerical noise [*Munk, 1950; Bryan et al., 1975; Large et al., 2001*].  
4 Isotropic viscosity schemes apply one large viscosity value needed for these purposes  
5 everywhere in the model which is not physically realistic outside of these specific areas. A  
6 major deficiency when using isotropic viscosities is the underestimation of the Pacific Equatorial  
7 Undercurrent which in models is typically about 10% compared to what is observed [*Large et*  
8 *al., 2001*]. The Pacific Equatorial Undercurrent is a source of relatively warm, fresh, nutrient-  
9 poor and oxygen-rich water from the Western Pacific that flows into the Eastern Pacific which  
10 has important physical and biogeochemical effects. We implement an anisotropic viscosity  
11 scheme similar to *Large et al. [2001]* in the tropics to better resolve equatorial dynamics. Figure  
12 S1-1 shows zonal and meridional surface viscosities used and Figure S1-2 shows a comparison at  
13 125°W of the simulated currents with observations in the Eastern Tropical Pacific [*Kessler,*  
14 *2006*], the region most significantly affected by the anisotropic viscosity scheme.

15

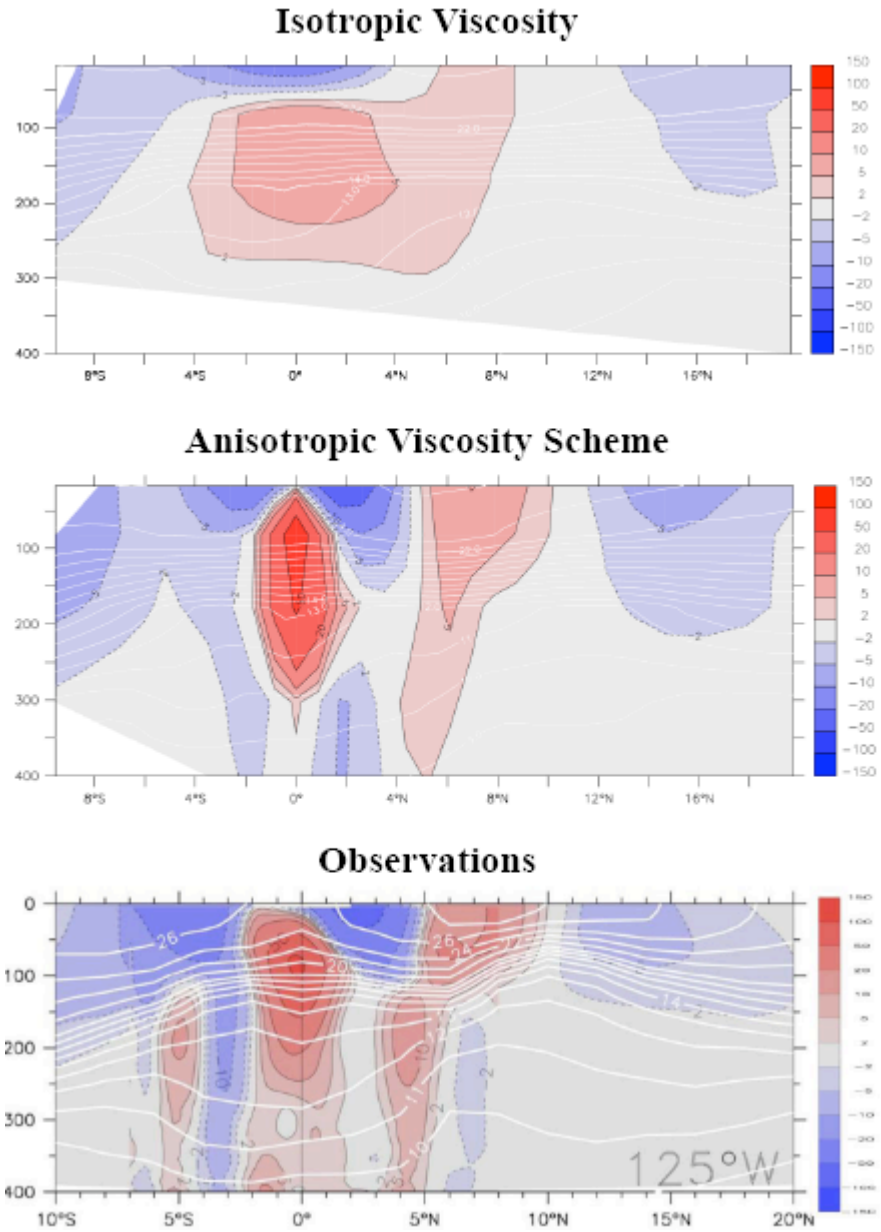


16

17

18 **Figure S1-1.** Surface viscosity in the meridional and zonal directions.

19



20

21

22 **Figure S1-2.** Annual averaged zonal velocity ( $\text{cm s}^{-1}$ ) along  $125^\circ\text{W}$  using (a) an isotropic  
 23 viscosity, (b) the anisotropic viscosity scheme and (c) observations from *Kessler [2006]*.

24

## 24 **Supplementary Material 2: Marine Ecosystem Model**

25 This appendix provides a description of the parameters used in the full set of time-dependent  
26 equations in the marine ecosystem model. It suffices to note that the equations for total nitrogen  
27 ( $^{14}\text{N} + ^{15}\text{N}$ ) ecosystem variables are identical to the ones of  $^{15}\text{N}$  if  $R_X = \beta_X/(1+\beta_X) = 1$ , which are  
28 located in Appendix A.

29

30 The function  $J_O$  provides the growth rate of non-diazotrophic phytoplankton, determined  
31 from irradiance ( $I$ ),  $\text{NO}_3^-$  and  $\text{PO}_4^{3-}$ ,

32

$$33 \quad J_O(I, \text{NO}_3^-, \text{PO}_4^{3-}) = \min(J_{OI}, J_{Omax}u_N, J_{Omax}u_P) \quad (\text{S2-1})$$

34

35 The maximum growth rate is dependent only on temperature (T):

36

$$37 \quad J_{Omax} = a \cdot \exp(T/T_b) \quad (\text{S2-2})$$

38

39 such that growth rates increase by a factor of ten over the temperature range of -2 to 34 °C. We  
40 use  $a=0.11 \text{ d}^{-1}$  for the maximum growth rate at 0 °C which was determined to optimize surface  
41 nutrient concentrations. Under nutrient-replete conditions, the light-limited growth rate  $J_{OI}$  is  
42 calculated according to:

43

$$44 \quad J_{OI} = \frac{J_{Omax} \alpha I}{[J_{Omax}^2 + (\alpha I)^2]^{1/2}} \quad (S2-3)$$

45

46 where  $\alpha$  is the initial slope of the photosynthesis vs. irradiance (P-I) curve. The calculation of the  
47 photosynthetically active shortwave radiation  $I$  and the method of averaging equation (S2-3) over  
48 one day is outlined in *Schmittner et al.* [2005]. This version also includes in the correction for  
49 the error in the calculation of light limitation in previous versions [*Schmittner et al.*, 2008b].  
50 Nutrient limitation is represented by the product of  $J_{Omax}$  and the nutrient uptake rates,  $u_N =$   
51  $NO_3^- / (k_N + NO_3^-)$  and  $u_P = PO_4^{3-} / (k_P + PO_4^{3-})$ , with  $k_P = k_N R_{P:N}$  providing the respective  
52 nutrient uptake rates.

53

54 Diazotrophs grow according to the same principles as the general phytoplankton class, but are  
55 disadvantaged in nitrate-bearing waters by a lower maximum growth rate,  $J_{Dmax}$ , which is set to  
56 zero below 15°C:

57

$$58 \quad J_{Dmax} = c_D \max[0, a(\exp(T / T_b) - 2.61)] \quad (S2-4)$$

59

60 The coefficient  $c_D$  handicaps diazotrophs by dampening the increase of their maximal growth  
61 rate versus that of the general phytoplankton class with rising temperature. We use  $c_D = 0.5$ , such

62 that the increase per °C warming of diazotrophs is 50% that of other phytoplankton. This  
63 handicap is further decreased to  $c_D = 0.25$  when aeolian dissolved Fe deposition is below 10  
64  $\mu\text{mol Fe m}^2 \text{ yr}^{-1}$  [Fan *et al.*, 2006] and smoothly transitions to  $c_D = 0.5$  outside of these areas.  
65 However, diazotrophs have an advantage in that their growth rate is not limited by  $\text{NO}_3^-$   
66 concentrations:

67

$$68 \quad J_D(I, PO_4) = \min(J_{DL}, J_{Dmax}\mu_P) \quad (\text{S2-5})$$

69

70 although they do take up  $\text{NO}_3^-$  if it is available (see term 5 in the right hand side of eq. C10). The  
71 N:P of model diazotrophs is equal to the general phytoplankton class (16:1). Although there is  
72 evidence that the best-studied diazotrophs of the genus *Trichodesmium* have much higher N:P  
73 [e.g. Sanudo-Wilhelmy *et al.*, 2004], the more abundant unicellular diazotrophs are  
74 uncharacterized [Karl *et al.*, 2002] and for simplicity of interpretation we opted to keep the N:P  
75 of both phytoplankton groups identical.

76

77 The first order mortality rate of phytoplankton is linearly dependent on their concentration,  $P_O$ .  
78 DOM and the microbial loop are folded into a single fast-remineralization process, which is the  
79 product of  $P_O$  and the temperature dependent term

80

$$81 \quad \mu_P = \mu_{PO} \exp(T / T_b). \quad (\text{S2-6})$$

82

83 Diazotrophs die at a linear rate where half of the resulting detritus is included into the fast-  
84 remineralization process.

85

86 Grazing of phytoplankton by zooplankton is unchanged from *Schmittner et al.* [2005]. Detritus is  
87 generated from sloppy zooplankton feeding and mortality among the three classes of plankton,  
88 and is the only component of the ecosystem model to sink. It does so at a speed of

89

$$w_D = \begin{cases} w_{D0} + m_w z, z \leq 1000m \\ w_{D0} + m_w 1000m, z > 1000m \end{cases}, \quad (\text{S2-7})$$

91

92 increasing linearly with depth  $z$  from  $w_{D0}=7 \text{ md}^{-1}$  at the surface to  $40 \text{ md}^{-1}$  at 1 km depth and  
93 constant below that, consistent with observations [*Berelson, 2002*]. The remineralization rate of  
94 detritus is temperature dependent and decreases by a factor of 5 in suboxic waters, as  $O_2$   
95 decreases from  $5 \mu\text{M}$  to  $0 \mu\text{M}$ :

96

$$\mu_D = \mu_{DO} \exp(T / T_b) [0.65 + 0.35 \tanh(O_2 - 6)] \quad (\text{S2-8})$$

98

99 Remineralization transforms the N and P content of detritus to  $\text{NO}_3^-$  and  $\text{PO}_4^{3-}$ . Photosynthesis  
100 produces oxygen, while respiration consumes oxygen, at rates equal to the consumption and  
101 remineralization rates of  $\text{PO}_4$ , respectively, multiplied by the constant ratio  $R_{O:P}$ . Dissolved  
102 oxygen exchanges with the atmosphere in the surface layer ( $F_{sfc}$ ) according to the OCMIP  
103 protocol.

104

105 Oxygen consumption in suboxic waters ( $\text{O}_2 < \sim 5 \mu\text{M}$ ) is inhibited, according to

106

$$107 \quad r_{sox}^{O_2} = 0.5 [\tanh(O_2 - 5) + 1] \quad (\text{S2-9})$$

108

109 but is replaced by the oxygen-equivalent oxidation of nitrate,

110

$$111 \quad r_{sox}^{NO_3} = 0.5 [1 - \tanh(O_2 - 5)]. \quad (\text{S2-10})$$

112

113 Denitrification consumes nitrate at a rate of 80% of the oxygen equivalent rate, as  $\text{NO}_3$  is a more  
114 efficient oxidant on a mol per mol basis (i.e. one mol of  $\text{NO}_3$  can accept  $5e^-$  while 1 mol of  $\text{O}_2$   
115 can accept only  $4e^-$ ). Note that the model does not include sedimentary denitrification, which  
116 would provide a large and less time-variant sink for fixed nitrogen.



117

118 We implement the sedimentary denitrification metamodel equation of *Middleburg et al.* [1996]  
119 which parameterizes sedimentary denitrification based on the labile carbon flux ( $F_c$ ) into the  
120 sediments:

121

$$122 \quad \text{SedDeni} = \alpha_{SD} \times 10 \wedge \left[ -0.9543 + 0.7662 \times \log(F_c) - 0.2350 \times \log(F_c)^2 \right]$$

123 (S2-11)

124

125 SedDeni is the amount of  $\text{NO}_3^-$  that is removed from the bottom water. We assume that the flux  
126 of labile carbon ( $F_c$ ) occurs at a ratio of  $R_{C:N} = 6.6$  of the sinking nitrogen in the organic detritus.  
127 Because the continental shelves are not well resolved in the model, we use an additional  
128 parameterization for them. The portion of each ocean grid box that is covered by a shallower  
129 continental shelf is recorded as the SHELF coefficient. The labile organic carbon ( $F_c$ ) that is  
130 included in the sedimentary denitrification model in the shelf parameterization is the amount of  
131 organic carbon that sinks into the portion of the grid box covered by a shallower continental shelf  
132 (i.e.,  $\text{SHELF} \times F_c$ ). In the model, ~80% of the sedimentary denitrification occurs within this  
133 shelf parameterization. The remaining organic matter (i.e.,  $F_c \times [1 - \text{SHELF}]$ ) continues to sink  
134 to greater depths. The physical circulation model's inability to fully resolve coastal upwelling  
135 systems also underestimates primary production and sinking carbon fluxes on the continental  
136 shelves and hence sedimentary denitrification. To account for this, we arbitrarily multiply the  
137 sedimentary denitrification rate by a coefficient  $\alpha_{SD}$  tuned to 6.5 to set the global deep oceanic

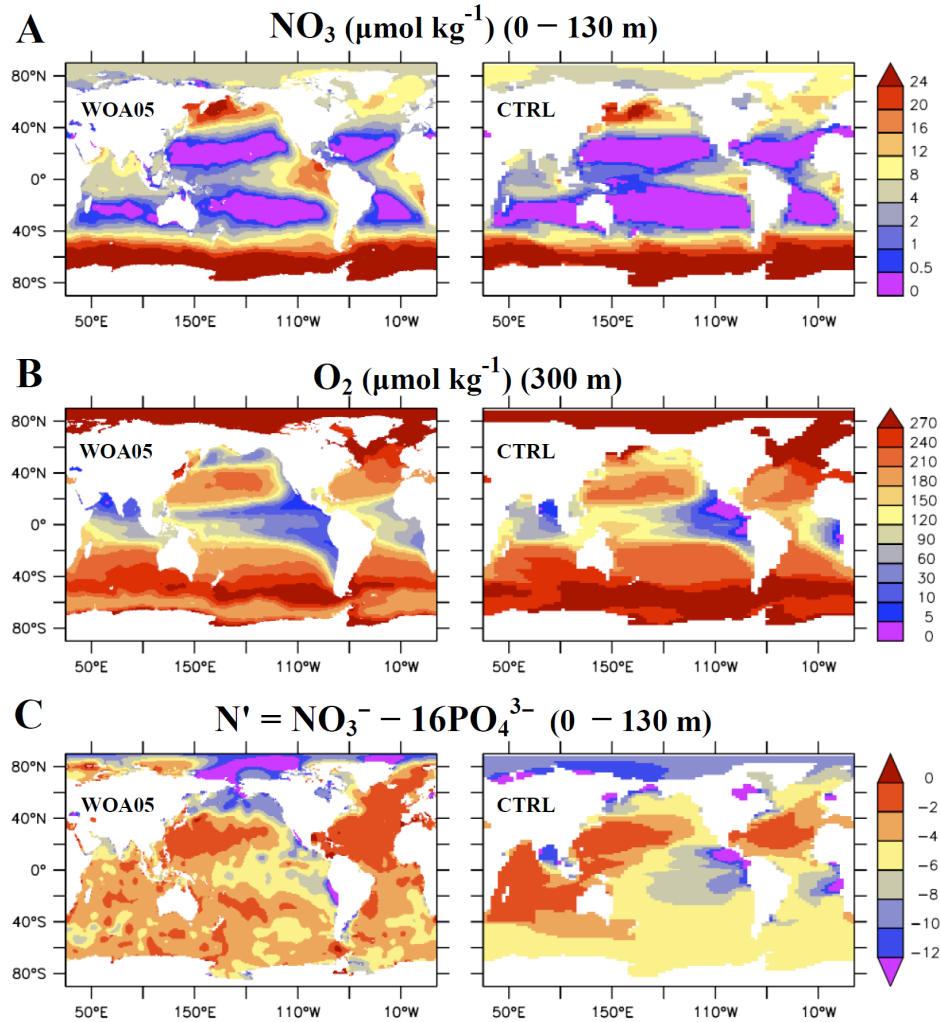
138  $\delta^{15}\text{NO}_3$  average in the model to  $\sim 5\%$ . Without this parameterization, the deep oceanic  $\delta^{15}\text{NO}_3$   
139 average slowly drifts well above  $10\%$ . The tuning parameter  $\alpha_{\text{SD}}$  was also tested at the values of  
140 6 and 7, which resulted in deep oceanic  $\delta^{15}\text{NO}_3$  averages of  $5.2\%$  and  $4.95\%$ , respectively.  
141 Figure 2 shows the spatial distribution of sedimentary denitrification.

<i>Parameter</i>	<i>Symbol</i>	<i>Value</i>	<i>Units</i>
<i>Phytoplankton (P<sub>O</sub>, P<sub>D</sub>) Coefficients</i>			
Initial slope of P-I curve	$\alpha$	0.1	$(\text{W m}^{-2})^{-1} \text{d}^{-1}$
Photosynthetically active radiation	$PAR$	0.43	
Light attenuation in water	$k_w$	0.04	$\text{m}^{-1}$
Light attenuation through phytoplankton	$k_c$	0.03	$\text{m}^{-1}(\text{mmol m}^{-3})^{-1}$
Light attenuation through sea ice	$k_i$	5	$\text{m}^{-1}$
Maximum growth rate	$a$	0.2	$\text{d}^{-1}$
Half-saturation constant for N uptake	$k_N$	0.7	$\text{mmol m}^{-3}$
Specific mortality rate	$\mu_P$	0.05	$\text{d}^{-1}$
Fast recycling term (microbial loop)	$\mu_{P0}^*$	0.04	$\text{d}^{-1}$
Diazotrophs' handicap	$c_D$	0.5	
<i>Zooplankton (Z) Coefficients</i>			
Assimilation efficiency	$\gamma_l$	0.925	
Maximum grazing rate	$g$	1.575	$\text{d}^{-1}$
Prey capture rate	$\varepsilon$	1.6	$(\text{mmol m}^{-3})^{-2} \text{d}^{-1}$
Mortality	$\mu_Z$	0.34	$(\text{mmol m}^{-3})^{-2} \text{d}^{-1}$

<i>Parameter</i>	<i>Symbol</i>	<i>Value</i>	<i>Units</i>
Excretion	$\gamma_2$	0.05	d <sup>-1</sup>
<i>Detritus (D) Coefficients</i>			
Remineralization rate	$\mu_{D0}$	0.048	d <sup>-1</sup>
Sinking speed at surface	$w_{D0}$	7	m d <sup>-1</sup>
Increase of sinking speed with depth	$m_w$	0.04	d <sup>-1</sup>
E-folding temperature of biological rates	$T_b$	15.65	°C
<i>Other Coefficients</i>			
Molar elemental ratios	$R_{O:N}$	10.6	
	$R_{N:P}$	16	

143 **Table S2-1:** Marine Ecosystem Parameters.

144



144

145 **Figure S2-1.** Top Panel: Comparison between annual WOA05 observations [*Garcia et al.*,  
 146 2006] with CTRL of (A) surface  $\text{NO}_3$ , (B) subsurface  $\text{O}_2$ , and (C) surface  $\text{N}'$ .

147

148